

## Influence of contact area on memristive characteristics of parylene-based structures in single and crossbar geometry

© B.S. Shvetsov,<sup>1,2</sup> G.A. Iukliaevskikh,<sup>2</sup> K.Yu. Chernoglazov,<sup>1</sup> A.V. Emelyanov<sup>1</sup>

<sup>1</sup> National Research Center „Kurchatov Institute“,  
123098 Moscow, Russia

<sup>2</sup> Moscow State University,  
119991 Moscow, Russia

e-mail: b.shvetsov15@physics.msu.ru

Received July 4, 2023

Revised September 20, 2023

Accepted September 25, 2023

The key elements of neuromorphic computing systems (NCS) are memristors — resistors with a memory effect — that can be used for simultaneous processing and storage of information. It is promising to create them in crossbar geometry, where memristors are located at the intersections of the transverse electrode buses. In this work, the influence of the area and geometry of contacts on the main memristive characteristics of parylene-based structures is investigated. The results obtained indicate the independence of such memristive characteristics as the switching voltage into the low-resistance ( $U_{\text{set}}$ ) and high-resistance states ( $U_{\text{reset}}$ ), as well as the resistance of the samples in the low-resistance ( $R_{\text{on}}$ ) state, from the contact area. At the same time, resistances in the high-resistance ( $R_{\text{off}}$ ) state increase with decreasing area, which confirms the single-filament model of resistive switching, and also makes it possible to increase the window of resistance in such structures.

**Keywords:** memristors, resistive switching, neuromorphic systems, parylene.

DOI: 10.61011/TP.2023.11.57500.166-23

### Introduction

Recently, extensive investigations for creation of new neuromorphic computing systems (NCS) have been being carried out [1,2]. This is due to the fact that neural networks based on the classical von Neumann architecture feature high energy consumption and low performance. One of approaches to solve this problem is to design brand new devices whose architecture is based on neural connectivity in biological systems [3]. Such hardware-implemented neural networks are referred to as NCS [4]. Memristor, a resistor with memory effect that can be used for simultaneous data processing and storage [5–9], has good prospects of application in such networks. Its operating principle is based on the resistive switching (RS) effect under the applied electric field [10]. Due to such principle, memristors may have several resistive states and store the pre-defined resistive state after release of the electric field. These properties allow to use memristors in NCS as synapse equivalents to connect neurons in biological systems and function as memory cells [11].

The RS phenomenon was found in structures based both on organic [12] and inorganic [13] materials. Development of memristive structures based on inorganic materials was initially a more popular area due to their compatibility with silicon technologies. However, the interest in the investigation of memristors based on organic materials has grown recently, because they are as good as inorganic materials in their main properties: resistance ratio in high-resistance and low-resistance states, cyclic switchings

without degradation, resistive state storage time, plasticity (number and hold time of resistive states), etc. [14,15]. In addition, structures based on organic materials are low-cost, sufficiently easy-to-produce and biocompatible. It should be noted that flexible substrate memristors may be created using organic materials [16,17]. Currently, poly-p-xylylene (Parylene, PPX) is one of the most promising organic materials [17–19].

Single PPX-based capacitor structures show good memristive characteristics, however, crossbar geometry, a set of electrode crossbars interlaid with dielectric, shall be used in NCS [20]. In such structures, memristors at crossbar intersections play a role of NCS synaptic scales. Formal NCS may be built using crossbar arrays, since they may be used to easily multiply the incoming pulses by the synaptic scaling matrix according to laws of physics (Ohm's law and Kirchhoff's law). In such structures, data is stored and processed directly in memory cells, therefore they feature high energy performance. Crossbar arrays provide a wide range of options in decision-making, photo and video recognition, drone operation applications, etc. For PPX-based memristive structures, dependences of resistances in low- and high-resistance states on the contact areas have not been studied before. At the same time, such studies are important for understanding the resistive switching mechanism in such structures and the scalability, in particular in the crossbar geometry. Therefore, the purpose of this study was to investigate the effect of contact area and geometry on the main memristive characteristics.

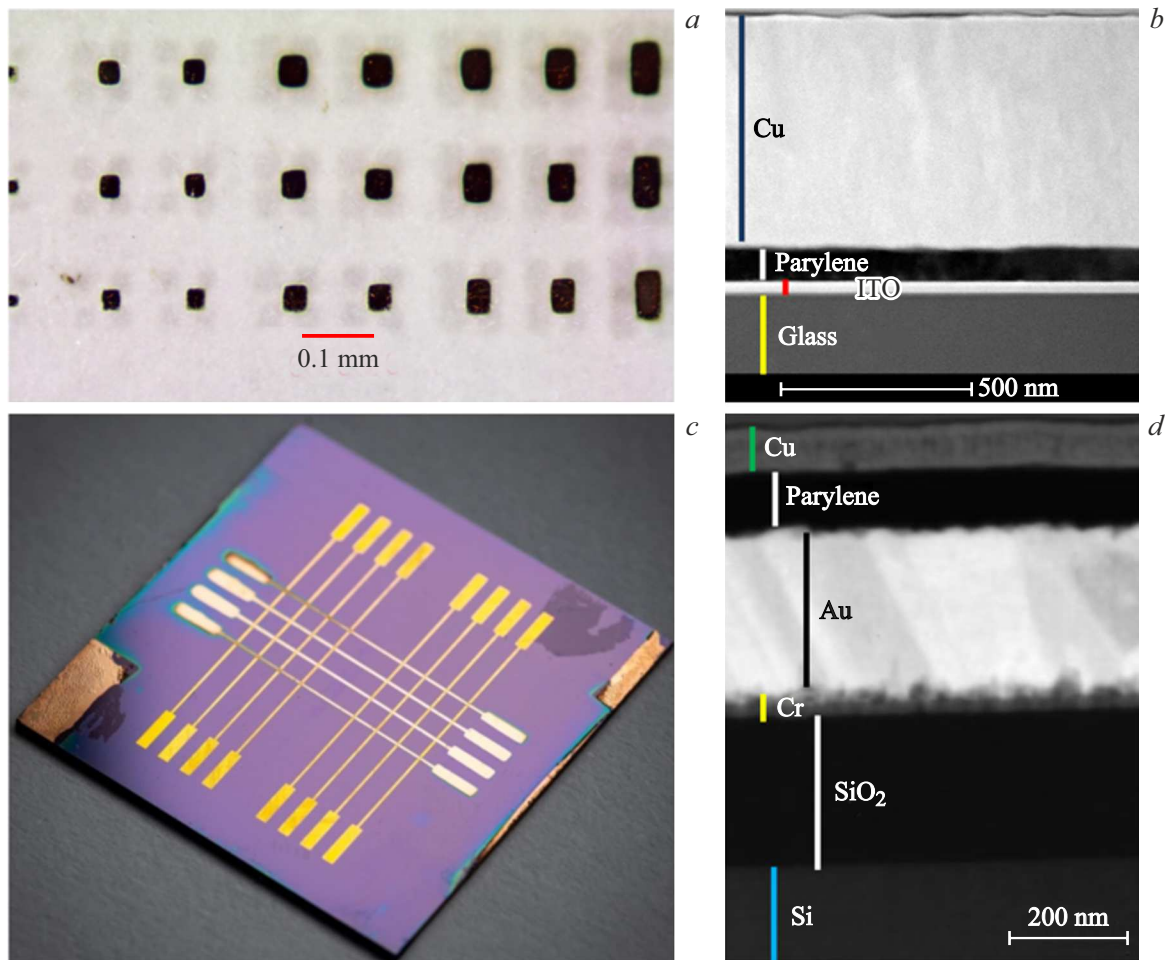


**Figure 1.** Single Cu/PPX/ITO memristive structures with various areas (*a*); TEM image of a Cu/PPX/ITO structure (*b*); Cu/PPX/Au memristor crossbar arrays (*c*); TEM image of a Cu/PPX/Au structure (*d*).

## 1. Materials and methods

Cu/PPX/ITO memristive structures in single-capacitor geometry were studied (Figure 1, *a*). A  $\sim 100$  nm PPX layer was applied to a glass substrate with applied ITO (indium–tin oxide), that was used as a bottom electrode, by the gas-phase surface initiated polymerization method using SCS Labcoater PDS 2010 vacuum deposition system. The deposition uses a vacuum level sufficient for uniform deposition of gaseous monomer to cover the whole surface. Top metal electrodes consisted of  $\sim 500$  nm copper (Cu) layers applied by shadow-mask magnetron sputtering. Samples with different active electrode areas were made:  $S_1 = 1 \text{ mm}^2$ ,  $S_2 = 0.2 \text{ mm}^2$ ,  $S_3 = 0.1 \text{ mm}^2$ ,  $S_4 = 0.08 \text{ mm}^2$ . Copper was chosen as the top electrode, because this material has demonstrated the best electro-physical properties in similar memristive structures [14]. transmission electron microscopy (TEM) image of single test samples is shown in Figure 1, *b*.

Crossbar-geometry Cu/PPX/Au memristor arrays were also studied (Figure 1, *c*). Memristors were made on  $\text{SiO}_2/\text{Si}$  substrates previously coated with a  $\text{Si}_3\text{N}_4$  layer. To

apply the bottom gold electrode (280 nm) on a chromium sublayer (30 nm), a photolithography method was used (for details see [21]). Then a  $\sim 100$  nm PPX layer was applied by the gas-phase surface initiated polymerization. Then a copper layer was applied by the shadow-mask magnetron sputtering method. Samples with various bottom contact areas ( $20, 100, 150 \mu\text{m}$ ) were made. Areas of these samples were, respectively, equal to  $S_{150} = 0.026 \text{ mm}^2$  (copper contact width was  $170 \mu\text{m}$ ),  $S_{100} = 0.031 \text{ mm}^2$  (copper contact width was  $310 \mu\text{m}$ ),  $S_{20} = 0.005 \text{ mm}^2$  (copper contact width was  $250 \mu\text{m}$ ). TEM image of a crossbar array with a  $20 \mu\text{m}$  gold crossbar is shown in Figure 1, *d*.

Memristive properties of Cu/PPX/ITO and Cu/PPX/Au structures (switching voltages  $U_{\text{set}}$ ,  $U_{\text{reset}}$ , low-resistance and high-resistance state resistances  $R_{\text{on}}$  and  $R_{\text{off}}$ , resistive state hold times and number of resistive states) were studied using Economic 4'' Probe Station (EPS4). Voltage pulses were applied to the top electrode with grounded bottom electrode from Keithley 2636B sourcemeter programmed in LabVIEW. All measurements were performed at room temperature.

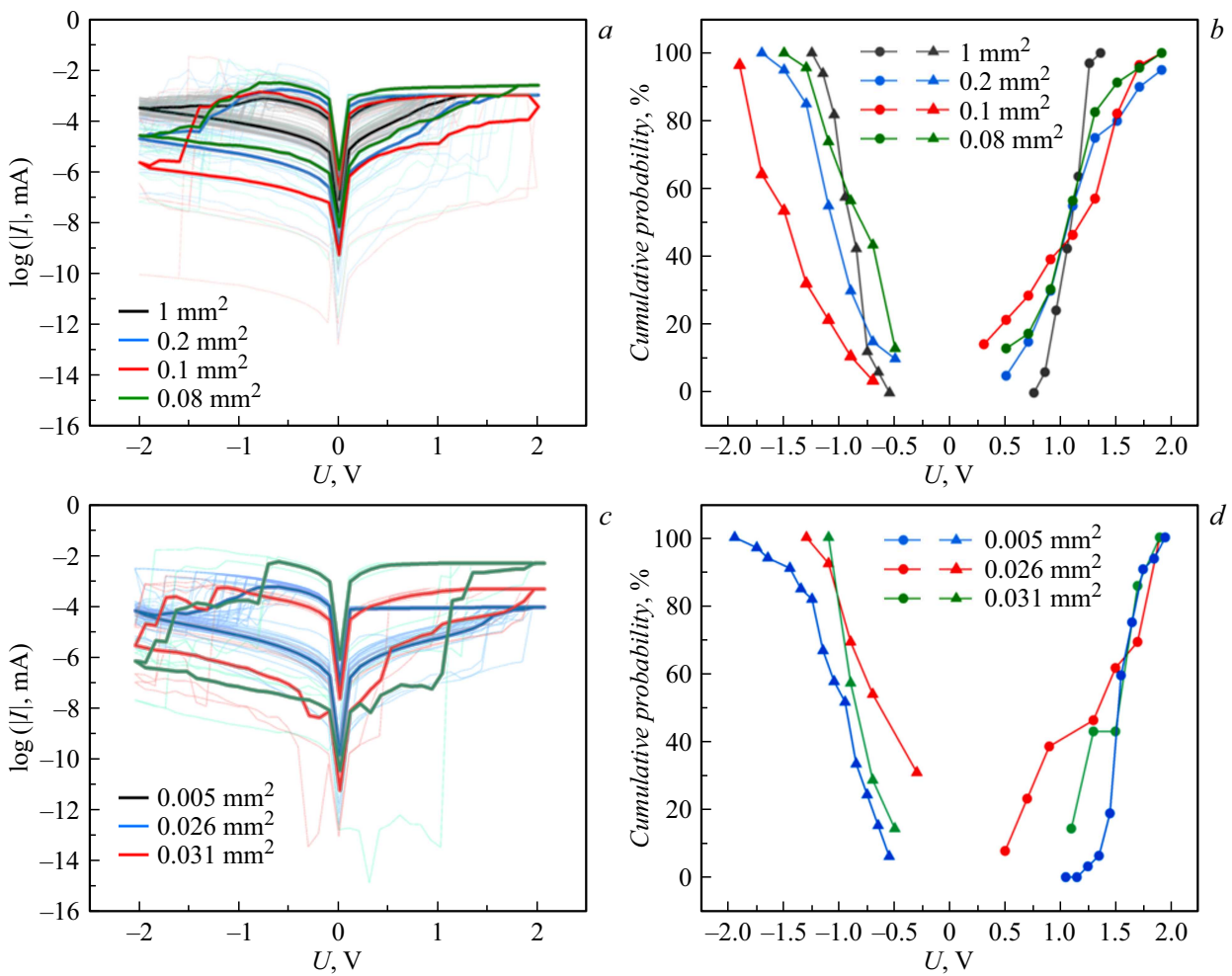


**Figure 2.** Current-voltage curves ( $I$ – $V$  curves) for Cu/PPX/ITO samples (a) and their cumulative probabilities (b);  $I$ – $V$  curves for Cu/PPX/Au samples (c) and their cumulative probabilities (d).

**Table 1.** Average switching voltages of single samples for each contact area

Contact area	1 mm <sup>2</sup>	0.2 mm <sup>2</sup>	0.1 mm <sup>2</sup>	0.08 mm <sup>2</sup>
$U_{set}, V$	1.1 ± 0.1	1.1 ± 0.5	1.1 ± 0.5	1.1 ± 0.4
$U_{reset}, V$	–0.9 ± 0.2	–0.8 ± 0.4	–0.7 ± 0.4	–0.7 ± 0.3

## 2. Results and discussion

Figure 2, a shows semilogarithmic-scale current-voltage curves ( $I$ – $V$  curves) for four areas of single samples. Each  $I$ – $V$  curves was measured by applying voltage  $U$  in the following sequence: time-linear voltage increase from zero to positive threshold value  $U_+$ , then decrease to negative threshold value  $U_-$  and then increase to zero. Voltage varied from 2 to –2 V with an increment of 0.1 V. The current was limited within [–50, 1] mA to prevent structure overheating and degradation. A heavy line shows averaging of the obtained  $I$ – $V$  curves.  $I$ – $V$  curves were used to determine voltages of switching to low-resistance state ( $U_{set}$ ) and high-resistance state ( $U_{reset}$ ):  $U_{set}$  meant the voltage at

which positive threshold current was achieved,  $U_{reset}$  meant the voltage at which differential resistance sign reversal took place in the negative voltage region. The obtained switching voltages  $U_{set}$  and  $U_{reset}$  averaged by at least 5 cycles for each area are shown in Table 1. Figure 2, b shows cumulative probabilities of state switching voltages  $U_{reset}$  and  $U_{set}$  for four areas of single samples. The diagram shows that the voltage dispersion for switching to the low-resistance state is the same for all areas and for switching to the high-resistance state is a little different. This may be attributed to the fact that PPX width varies from sample to sample by some nanometers.

Figure 2, c shows the curves that demonstrate semilogarithmic  $I$ – $V$  curves for three areas of memristor crossbar

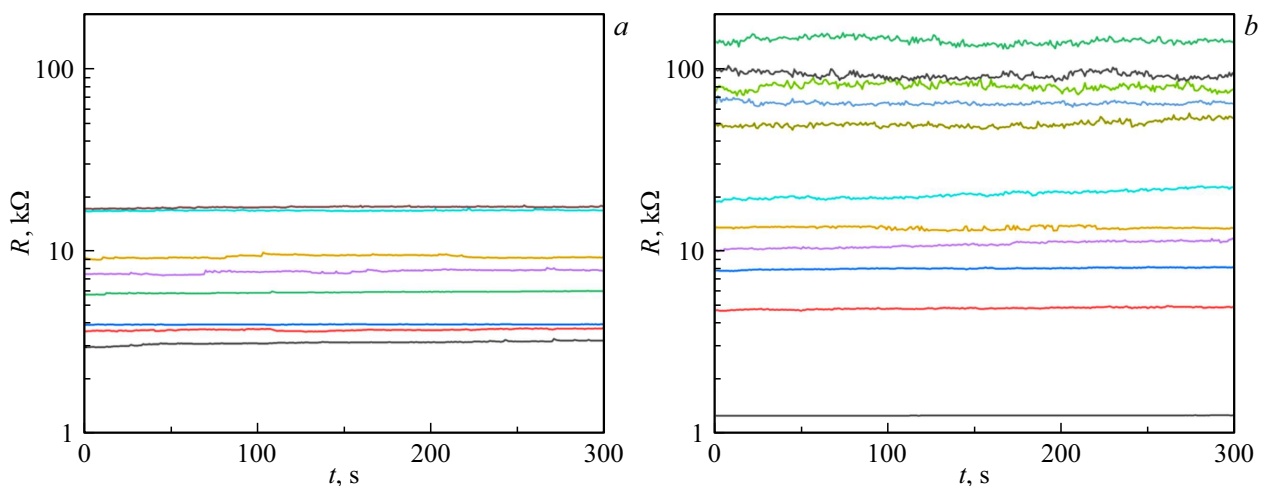


**Figure 3.** Stable resistive states for single Cu/PPX/ITO samples  $1 \text{ mm}^2$  in area (a) and for Cu/PPX/Au crossbar samples  $0.005 \text{ mm}^2$  in area (b).

arrays. Voltage varied from 2 to  $-2 \text{ V}$  with an increment of  $0.1 \text{ V}$ . The current was limited within  $[-5, 0.5] \text{ mA}$  to prevent structure overheating and degradation. Different limiting current was used for different areas, because structures with smaller area degraded faster at the maximum current and switching was not observed. A heavy line shows averaging of the obtained I–V curves. Figure 2, d shows cumulative probabilities of switching to the high-resistance and low-resistance states for three areas of memristor crossbar arrays. It should be noted that leakage currents are of great concern in passive crossbar architectures [22,23]. To avoid this problem, either special architectures (with transistor or selector) or special reading circuits are used such as unselected electrode grounding or so-called V/2 or V/3 circuits [22,23]. The first option requires complex processes that are not addressed herein, and the second option results in increased power consumption. Herein, after using each memristor in a crossbar, it remained in state  $R_{\text{off}}$ , therefore, the occurring leakage currents were minimized. However, the obtained memristive properties were not dependent on the memristor location in the crossbar (I–V curves dispersion for different memristors in the crossbar matrix is not higher than that for a single memristor from cycle to cycle) suggesting low influence of leakage currents on the obtained properties.

In the same way as for single samples, average switching voltages were calculated. The results are shown in the Table 2. As shown in the Table, high-resistance and low-resistance switching voltages are the same for different areas taking into account the error.

In addition, multilevel RS of memristive structures with areas  $S_1 = 1 \text{ mm}^2$  and  $S_{20} = 0.005 \text{ mm}^2$  were investigated as extreme values from the examined area range (Figure 3). To achieve a stable resistive state,  $100 \text{ ms}$  pulses were applied to the structure, the pulse amplitude was growing with an increment of  $0.1 \text{ V}$  until switching to the pre-defined state occurred. When the required resistive state had been

**Table 2.** Average switching voltages of crossbar arrays for each contact area

Contact area	$0.005 \text{ mm}^2$	$0.026 \text{ mm}^2$	$0.031 \text{ mm}^2$
$U_{\text{set}}, \text{ V}$	$1.5 \pm 0.3$	$1.3 \pm 0.6$	$1.5 \pm 0.3$
$U_{\text{reset}}, \text{ V}$	$-1.1 \pm 0.4$	$-0.9 \pm 0.4$	$-0.8 \pm 0.2$

achieved, a reading pulse with a reading voltage of  $0.1 \text{ V}$  was applied to provide the sample resistance data [24]. Figure 3, a shows 8 stable resistive states for  $S_1 = 1 \text{ mm}^2$  of a single sample, with each of them stored for at least 300 s. Figure 3, b shows 10 stable resistive states for  $S_{20} = 0.005 \text{ mm}^2$  of a crossbar array sample, with each of them stored for at least 300 s. The curves show that with increasing area, the number of stable resistive states may be increased due to increasing resistance window  $R_{\text{off}}/R_{\text{on}}$ . Within the range of increasing  $R_{\text{off}}$  values for structures with smaller areas, several stable resistive states are identified (Figure 3, b). Apparently, this is caused by changed distance between open metal bridge ends.

The obtained data was used to draw a log-log scale curve of low-resistance and high-resistance state resistances vs. contact areas that is shown in Figure 4. As shown in the Figure, low-resistance state resistances (red dots (in online version)) retain their values at different areas. Slight differences may be attributed to different PPX layer thickness. At the same time, high-resistance state resistances (black dots) decrease with increasing area. Such behavior is explained by a single-filamentary RS model. According to this model, one or few filaments (metal bridges or conducting channels) are arranged throughout the contact area. Hence, the memristor resistance in the low-resistance state is defined by metal bridge parameters. When the contact area is changed, these parameters remain unchanged suggesting that there is no dependence of resistance on con-

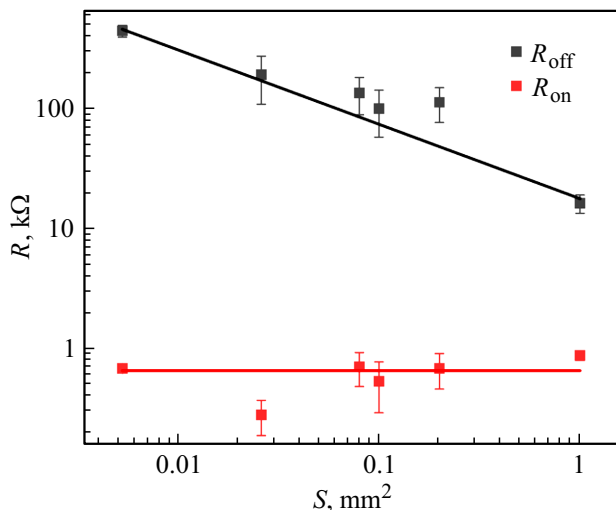


**Figure 4.** Dependence of low-resistance and high-resistance state resistances on contact areas.

tact area in the low-resistance state. In the high-resistance state, the metal bridge is open and the sample resistance depends on the parylene layer parameters. Therefore, log-log dependence  $R_{off} = f(S)$  is linear.

## Conclusion

Thus, the study investigated the effect of crossbar-geometry PPX-based memristor scaling on the main characteristics. It is shown that the switching voltage does not depend on the contact area. Independence of resistance in the low-resistance state on contact area was also detected. However, the memristor resistance in the high-resistance state was inversely proportional to the contact area. All these results indicate that a single-filamentary type of resistive switching is implemented for the examined memristive structures.

The findings offer opportunities for downward scaling of memristive device sizes in order to increase the number of memristive devices per unit area. Prospects of this study are associated with NCS performance growth and with formal neural networking using crossbar-geometry PPX-based memristors.

## Funding

This study was funded by the Ministry of Science and Higher Education of the Russian Federation under Agreement № 075-15-2021-1357 using the equipment of the Resource Centers (SRC „Kurchatov Institute“).

## Acknowledgments

The authors are grateful to A.A. Nesmelov and Yu.V. Grishchenko (SRC „Kurchatov Institute“) for the assistance in sample preparation.

## Conflict of interest

The authors declare that they have no conflict of interest.

## References

- [1] D. Kuzum. *IEEE Nanotechnol. Mag.*, **12**, 4 (2018).
- [2] J. Zhu, T. Zhang, Y. Yang, R. Huang. *Appl. Phys. Rev.*, **7**, 011312 (2020). <https://doi.org/10.1063/1.5118217>
- [3] Z. Wang, H. Wu, G.W. Burr, C.S. Hwang, K.L. Wang, Q. Xia, J.J. Yang. *Nat. Rev. Mater.*, **5**, 173 (2020).
- [4] Q. Xia, J.J. Yang. *Nat. Mater.*, **18**, 309 (2019).
- [5] K. Berggren, Q. Xia, K.K. Likharev, D.B. Strukov, H. Jiang, T. Mikolajick, D. Querlioz, M. Salinga, J.R. Erickson, S. Pi, F. Xiong, P. Lin, C. Li, Y. Chen, S. Xiong, B.D. Hoskins, M.W. Daniels, A. Madhavan, J.A. Liddle, J.J. McClelland, Y. Yang, J. Rupp, S.S. Nonnenmann, K.-T. Cheng, N. Gong, M.A. Lastras-Montañó, A.A. Talin, A. Salleo, B.J. Shastri, T.F. de Lima, P. Prucnal, A.N. Tait, Y. Shen, H. Meng, C. Roques-Carmes, Z. Cheng, H. Bhaskaran, D. Jariwala, H. Wang, J.M. Shainline, K. Segall, J.J. Yang, K. Roy, S. Datta, A. Raychowdhury. *Nanotechnology*, **32**, 012002 (2021).
- [6] A.A. Koroleva, M.G. Kozodaev, Y.Y. Lebedinskii, A.M. Markeev. *Nanobiotechnology Reports*, **16** (6), 737 (2021). <https://doi.org/10.1134/S2635167621060094>
- [7] M.N. Koryazhkina, D.O. Filatov, S.V. Tikhov, A.I. Belov, D.S. Korolev, A.V. Kruglov, R.N. Kryukov, S.Y. Zubkov, V.A. Vorontsov, D.A. Pavlov, D.I. Tetelbaum, A.N. Mikhaylov, S. Kim. *Nanobiotechnology Reports*, **16** (6), 745 (2021). <https://doi.org/10.1134/S2635167621060100>
- [8] L.S. Parshina, D.S. Gusev, O.D. Khramova, A.S. Polyakov, N.N. Eliseev, O.A. Novodvorsky. *Nanobiotechnology Reports*, **16** (6), 829 (2021). <https://doi.org/10.1134/S2635167621060185>
- [9] A.N. Matsukatova, A.I. Iliasov, K.E. Nikiruy, E.V. Kukueva, A.L. Vasiliev, B.V. Goncharov, A.V. Sitnikov, M.L. Zhanavskin, A.S. Bugaev, V.A. Demin, V.V. Rylkov, A.V. Emelyanov. *Nanomaterials*, **12** (19), 3455 (2022). <https://doi.org/10.3390/nano12193455>
- [10] I. Valov, R. Waser, J.R. Jameson, M.N. Kozicki. *Nanotechnology*, **22**, 254003 (2011).
- [11] T. Shi, R. Wang, Z. Wu, Y. Sun, J. An, Q. Liu. *Small Struct.*, **2**, 2000109 (2021).
- [12] Y. Van De Burgt, A. Melianas, S.T. Keene, G. Malliaras, A. Salleo. *Nat. Electron.*, **1**, 386 (2018).
- [13] Y. Li, Z. Wang, R. Midya, Q. Xia, J. Joshua Yang. *J. Phys. D: Appl. Phys.*, **51**, 0 (2018).
- [14] A.A. Minnekhanov, A.V. Emelyanov, D.A. Lapkin, K.E. Nikiruy, B.S. Shvetsov, A.A. Nesmelov, V.V. Rylkov, V.A. Demin, V.V. Erokhin. *Sci. Rep.*, **9**, 10800 (2019).
- [15] A.A. Minnekhanov, B.S. Shvetsov, M.M. Martyshov, K.E. Nikiruy, E.V. Kukueva, M.Y. Presnyakov, P.A. Forsh, V.V. Rylkov, V.V. Erokhin, V.A. Demin, A.V. Emelyanov. *Org. Electron.*, **74**, 89 (2019).
- [16] B.S. Shvetsov, A.N. Matsukatova, A.A. Minnekhanov, A.A. Nesmelov, B.V. Goncharov, D.A. Lapkin, M.N. Martyshov, P.A. Forsh, V.V. Rylkov, V.A. Demin, A.V. Emelyanov. *Pis'ma v ZhTF* **45**, 40 (2019) (in Russian).
- [17] J.E. Kim, B. Kim, H.T. Kwon, J. Kim, K. Kim, D.W. Park, Y. Kim. *IEEE Access*, **10**, 109760 (2022).

- [18] Q. Chen, M. Lin, Z. Wang, X. Zhao, Y. Cai, Q. Liu, Y. Fang, Y. Yang, M. He, R. Huang. *Adv. Electron. Mater.*, **5**, 1800852 (2019).
- [19] A.N. Matsukatova, A.Y. Vdovichenko, T.D. Patsaev, P.A. Forsh, P.K. Kashkarov, V.A. Demin, A.V. Emelyanov. *Nano Res.*, **16**, 3207 (2023).
- [20] S. Gi, I. Yeo, M. Chu, S. Kim, B. Lee. *ISOCC 2015 — Int. SoC Des. Conf. SoC Internet Everything*, 215 (2016).
- [21] B.S. Shvetsov, A.A. Minnekhanov, A.V. Emelyanov, A.I. Ilyasov, Y.V. Grishchenko, M.L. Znaveskin, A.A. Nesmelov, D.R. Streltsov, T.D. Patsaev, A.L. Vasiliev, V.V. Rylkov, V.A. Demin. *Nanotechnology*, **33**, 255201 (2022).
- [22] Z. Tang, Y. Wang, Y. Chi, L. Fang. *Electronics*, **7**, 224 (2018).
- [23] V.A. Demin, I.A. Surazhevsky, A.V. Emelyanov, P.K. Kashkarov, M.V. Kovalchuk. *J. Comput. Electron.*, **19**, 565 (2020).
- [24] K.E. Nikiruy, A.V. Yemelyanov, V.A. Demin, V.V. Rylkov, A.V. Sitnikov, P.K. Kashkarov. *Pis'ma v ZhTF* **44**, 20 (2018) (in Russian).

*Translated by Ego Translating*